On-line rail defect diagnostics with differential eddy current probes and specific detection processing

Mohamed Bentoumi, Patrice Aknin, Gérard Bloch

EPJ manuscript No.
(will be inserted by the editor)

On-line rail defect diagnosis with differential eddy current probes and specific detection processing

by M. Bentoumi[1,2], P. Aknin[1], and G. Bloch[2]

[1] INRETS, 2 avenue Malleret-Joinville. 94114 Arcueil Cedex, France. e-mail: aknin@inrets.fr,
[2] CRAN (UMR CNRS 7039),ESSTIN, Rue Jean Lamour 54519 Vandoeuvre-les-Nancy Cedex, France. e-mail: bentoumi@esstin.uhp-nancy.fr, bloch@esstin.uhp-nancy.fr

the date of receipt and acceptance should be inserted later

Abstract. This paper presents a non destructive evaluation system for rail inspection with a device embedded in a subway train. The difficult operating conditions lead to the design of a specific double-coils and double-frequencies sensor that delivers 8 complementary signals. After the presentation of the technological solution, the paper deals with the detection of minor defects and presents three approaches: the first one is a time heuristic approach, the second one is based on wavelet basis projections, and the last one implements an inverse filtering which allows the transformation of the differential probe outputs into estimated absolute ones. The methods are validated statistically on a labeled defect data set with the help of ROC curves.

Key words. detection – differential probe – inverse filtering – Wiener filter – eddy currents – rail defect – wavelet

PACS. 06.90.+v Other topics in metrology, measurements, and laboratory procedures

1 The context of the application

The introduction of automatic driverless trains involves the redefinition of the whole traffic control system. Currently, the basic device of traffic control is the track circuit whose principal function is the train detection along a track section and secondary function is the detection of broken rail. This device will disappear in an automatic control context, and must be replaced by new means of broken rail detection. The frequency of rail breakage is weak, but its occurrence degrades immediately the quality of the complete transport system, of mechanical and electrical points of view (traction currents return to the electric substation through the rails).

This paper introduces a suitable differential eddy current sensor planned to replace the track circuit in its function of broken rail detection. An eddy current sensor is sensitive to any modification of the geometry and/or electromagnetic characteristics of the target. Obviously, transverse splits of the rail are detected, but minor defects as well (shelling, welded joints or corrugation for example). The detection and monitoring of these kinds of defect allow to set up predictive maintenance policy. This paper is focused on the detection procedures for minor defects.

2 The instrumentation and signal processing chain

Previous works led to the realization of a suitable double-coils and double-frequencies sensor [1]. The sensor structure was designed and optimized according to the following specifications: positioning at 40 mm height, vertical and horizontal displacements of the sensor due to the bogie dynamics and 100 km/h maximum speed of the train. Moreover a particular attention must be focused on strong acceleration levels (until $10g$) and electromagnetic compatibility problem caused mainly by the traction currents that circulate in the rails.

Two differential coils are used to ensure a greater immunity to the target-sensor distance variations for the detection of localized cracks as well as large shellings. The two supply frequencies make the sensor sensitive to the rail electromagnetic characteristics for different skin depths. After preprocessing, four complex channels (active and reactive parts) are available, which are equivalent to eight real signals $d_1(t)$, $d_2(t)$, ..., $d_8(t)$ (figure 1). The device thus generates complementary information that will be aggregated during the phase of defect recognition.

The digitalization is carried out with respect to the distance covered by the train with a fixed step dx of 5 mm. It must therefore be noted that, in all that follows, processed signals are discrete signals depending on distance

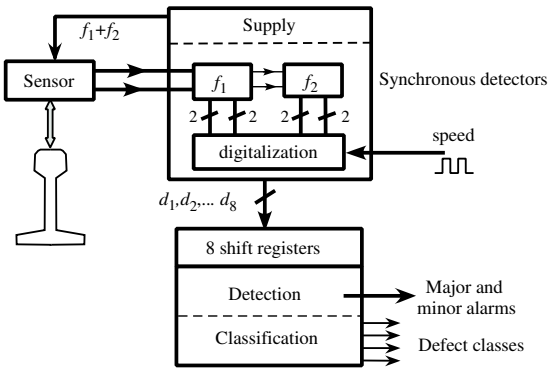

Fig. 1. data processing chain.

x. From these signals, a detection block finally generates major and minor alarms, and a classification module is activated if needed.

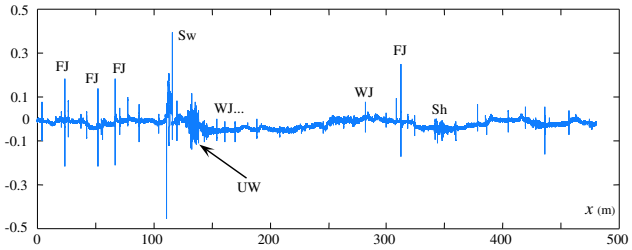

Fig. 2. example of signal d_1 evolution on 500 m track.

Figure 2 gives an example of the active part $d_1(x)$ on 500 m of rail. Particular points can be located, like switch (Sw), undulatory wear (UW) of the rail, fishplated joints (FJ), welded joints (WJ) and shellings (Sh).

After perusal of records, track visits are required, in order to precisely label each particular detected event. A series of tests led to gather about 600 defects distributed into four classes.

For on-line diagnosis, a detection (or segmentation) stage is required to isolate particular data segments on which a pattern recognition procedure can be applied.

The complexity of the processing lies in the fact that the track presents a great number of singularities which must be distinguished from the real defects. Furthermore, processing must be compatible with real time calculation capabilities of the system.

Three approaches for detection of minor defects (shellings, Sh, and welded joints, WJ) are presented. The first one is a time heuristic approach, the second one is based on wavelet basis projections, and the last one implements an inverse filtering which allows the transformation of the differential probe outputs into estimated absolute ones. The methods are validated statistically on the labeled defect data set with the help of ROC curves.

3 Heuristic time detection

3.1 Isochronism of differential signatures

As indicated previously, the sensor includes differential coils. A defect signature in the signals is directly related to an imbalance between the reluctances of the two associated windings. In the case of localized defect, the complete differential signature takes a symmetrical form with two successive swings, positive and negative (figure 3b). The equivalent frequency is proportional to the inner-distance of the differential coils.

Due to the bogie dynamics, the main source of errors lies in the rotating movements of the sensor relatively to the target (pitching). In this case, the reluctances of the elementary windings vary simultaneously (figure 3a). The signature is also symmetrical, but the equivalent frequencies are the same for the two differential coils, depending only on the natural frequency of the bogie and the speed of the train.

One solution to visualize the isochronism of the two signatures is to plot each signature with respect to one of the others into a pseudo-Lissajous plane (figure 3). In the case of pitching, the curve is roughly linear, whereas for a real defect the curve has two loops indicating the sequential run of the defect under the different windings.

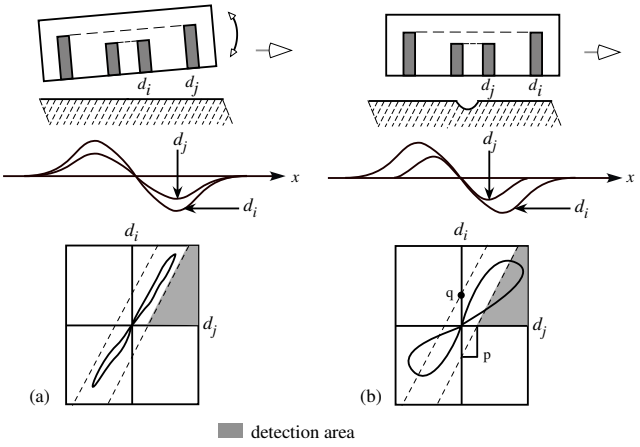

Fig. 3. effects of pitching (a) and defect (b).

A detector can be defined in such a plane, using linear decision boundaries, with threshold q and slope p (figure 3). As the sensor has four active channels with two different inner-distances, two distinct detectors can be built in planes $\{d_1, d_5\}$ and $\{d_3, d_7\}$. The fusion of these detectors is operated in a conjunctive way:

$$\begin{aligned}&[(d_5 < pd_1 - q) \cap (d_5 > 0)]\\ \cap&[(d_7 < pd_3 - q) \cap (d_7 > 0)] = 1\\ &\Longrightarrow minor\ defect\end{aligned} \quad (1)$$

3.2 The ROC Curve

This detection requires to tune the two parameters q and p of the boundary. The Receiver Operating Characteristic (ROC) was chosen to tune the detector. Well detection probabilities (Pw) are drawn according to the false detection probabilities (Pf) and the (0,1) point is the optimal operating point. These probabilities are estimated with the help of the experimental database built during in-site testing (435 minor defects). The nearest to the (0,1) point the ROC curve is, the better the tuning is.

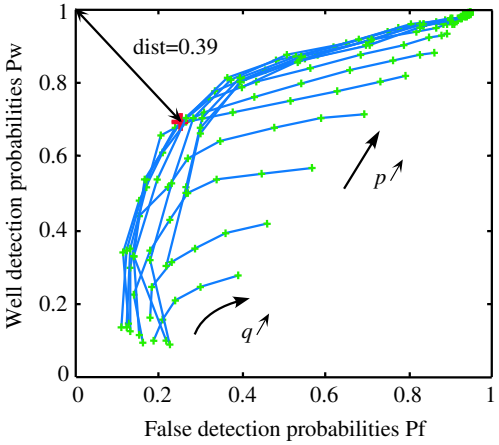

Fig. 4. ROC curves for heuristic detector.

Figure 4 presents ROC curves for 0.3 $<p<$ 10 and $0.001<q<0.1$. The optimal tuning is obtained with p=1 and q=0.008. However, the minimal distance to the (0,1) point remains relatively large ($dist\approx$0.39). Note that this detector is implemented after a bandpass filtering between 0.05 m and 2.5 m.

4 Detection in the time-scale plane

4.1 Choice of the mother wavelet and optimum scales

The second detector transposes the decision procedure in a transformed space. The transformation used is the continuous wavelet transform [2], applied to a complex space-dependent signal $f(x)$:

$$W[f](x,s) = \int_{-\infty}^{+\infty} f(t)\frac{1}{\sqrt{s}}\Psi^*(\frac{t-x}{s})dt \qquad (2)$$

where $\frac{1}{\sqrt{s}}\Psi(\frac{t-x}{s})$ is a version dilated with a scale parameter s and translated by a space-shift x of a function $\Psi(t)$ called "mother wavelet", such as $\int_{-\infty}^{+\infty}\Psi(t)dt = 0$, and Ψ^* stands for the complex conjugate of Ψ. Four continuous wavelet transforms are applied to the four eddy current channel outputs $d_{2i-1}(x) + jd_{2i}(x), i = 1,\ldots,4$:

$$W_i(x,s) = W[d_{2i-1}(x) + jd_{2i}(x)](x,s), \quad i = 1,\ldots 4 \quad (3)$$

The choice of the mother wavelet is important, particularly when the wavelet coefficients $W_i(x,s)$ are used as detectors. From a certain viewpoint, this kind of detection is close to adapted filtering [3]. The statistical defect base allows us to define a typical form of defect signature. Eight typical signatures (corresponding to the eight real signals) for each defect have been built by filtering and averaging the real defect signatures. Figure 5 shows two typical signatures of minor defects corresponding to the first channel (d_1(t), d_2(t)). A spline biorthogonal wavelet [2] has been chosen, its form being close to the differential minor defect signatures (figure 5).

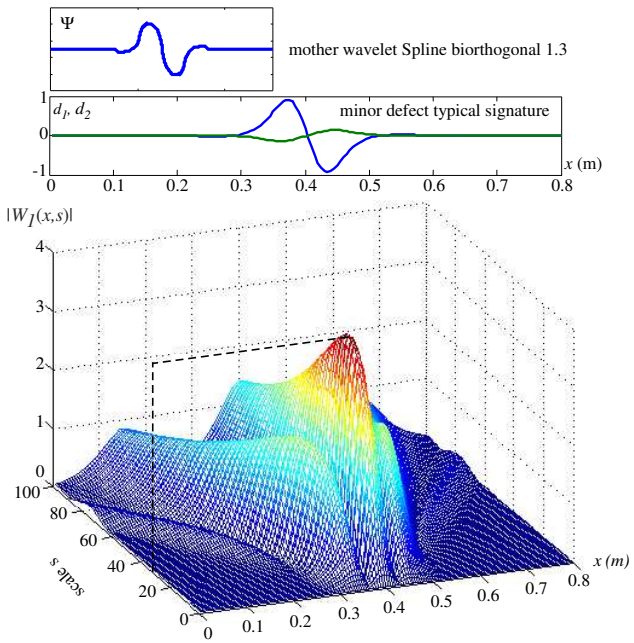

Fig. 5. mother wavelet, minor defect typical signature and wavelet transform.

Once the mother wavelet is chosen, the optimum scales $s_i, i = 1,\ldots,4$, must be determined. The modulus of the first wavelet transform, applied on minor defect typical signature, $W_1(x,s)$, corresponding to the first channel, is presented in figure 5. The higher the modulus is, the better the detection is. In this example, the highest modulus is obtained for scale value $s_1 = 27$. the optimal scale values for the four channels have been found equal to [27, 27, 39, 39]. The optimum scale mainly depends on the dimension of the differential coil arrangement (inner-distance between elementary coil).

4.2 Fusion of detectors

Each detector is dedicated to one coil and one frequency. Their redundancy can improve the robustness of the detection by aggregate them. For this purpose, the following total detector was built :

$$D(x) = \prod_{i=1}^{4} |W_i(x, s_i)| > Th \Rightarrow minor\ defect \quad (4)$$

where Th is the detection threshold.

Figure 6 presents an example of wavelet transform for the four channels and their multiplicative fusion.

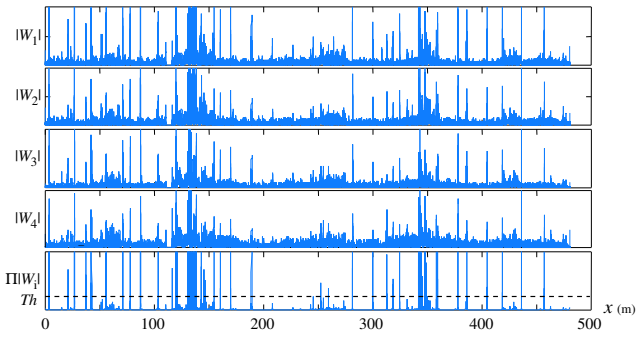

Fig. 6. fusion of wavelet detectors.

This multiplicative fusion increases the contrast between defect and no defect decisions. It can be referred to the evidence theory where belief masses are aggregated using the Dempster-Shaffer rule [4]. In the case of two exclusive classes (defect or no defect), nonstandard probabilistic fusion makes a normalized multiplication of the belief masses; here the normalization coefficient is equal to 1, indicating that no conflict exists between the detectors.

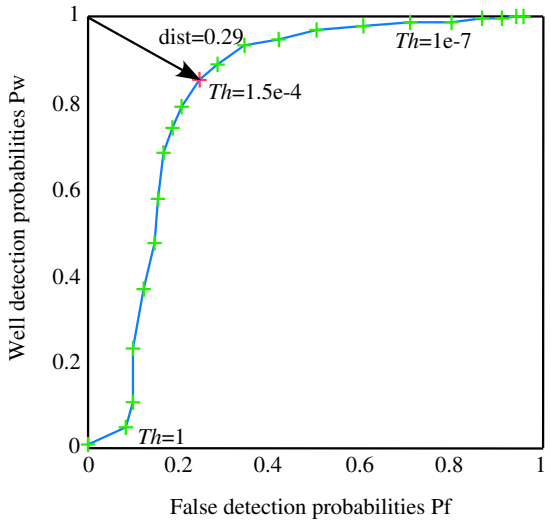

Fig. 7. ROC curve of the time-scale detector.

Figure 7 illustrates the tuning of the detector threshold with the help of ROC curve. The optimal value Th=1.5e-4 corresponds to the minimal distance $dist \approx 0.29$.

5 Inverse filtering

Differential probes allow relevant measurements in non-cooperative contexts such as modifications of target-sensor distance, variations of temperature, electromagnetic perturbations... However, the differential mode modifies the signal shape and its interpretation becomes more difficult.

The third detection procedure is built from estimated absolute signals, outcome of a deconvolution phase. First, the direct problem is introduced for differential measurements.

5.1 Direct model of single differential measurements

The principle of differential measurement is to subtract two close absolute measurements in order to constitute a local approximation of the absolute signal derivative. A compromise must be made between the quality of the derivative and the amplitude of the differential signal, both related to the inner-distance of the absolute coils (the smaller this distance is, the better the derivative quality is and the lower the differential signal amplitude is). The differential signal d is given by :

$$d(x) = a(x) - a(x - L) \quad (5)$$

where a is the absolute signal and x corresponds to a spatial variable. L is the inner-distance between the two absolute coils. An example of differential response is shown figure 8.

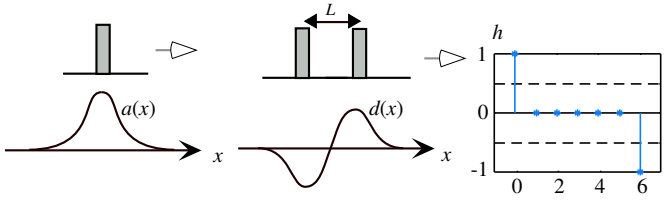

Fig. 8. impulse response of single differential measurements with ℓ=6.

The discrete version of equation (5) is:

$$d(i) = a(i) + a(i - \ell) \quad (6)$$

where $\ell = L/dx$ and dx is the sampling width. Equation (6) corresponds to a linear filtering with an impulse response h containing two opposite Dirac impulses separated by ℓ points (cf. figure 8).

In the general case of additive noise, the estimated absolute signal $\hat{a}$ is given by :

$$\hat{a} = g * (h * a) + g * b \quad (7)$$

where * denotes the convolution operation, a and b are respectively the absolute signal and the noise, h the impulse

response of the differentiation and g the impulse response of the inverse filter. The corresponding block diagram is given figure 9.

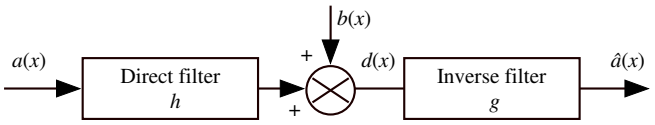

Fig. 9. principle of inversion.

The case of double-differential measurements can be taken up with the same approach [5].

5.2 Wiener filtering

Using for $G(j\omega)$ a direct inverse filter $1/H(j\omega)$ induces some problems. Indeed, a differential measurement cancels the harmonic components $1/L$, $2/L$, $3/L$... So the pure inverse filter has an infinite impulse response and becomes unusable in practice.

The inverse Wiener filter G minimizes the mean-square error between $a(x)$ and $\hat{a}(x)$, for a stationary context and uncorrelated signals. Its expression is based on Wiener-Hopf equation [6].

In the frequency domain, the signals $a(x)$ (absolute signal), $b(x)$ (noise) and $d(x)$ (differential signal) (cf. figure 9), of Fourier transforms $A(j\omega)$, $B(j\omega)$, $D(j\omega)$, have respectively $P_a(j\omega)$, $P_b(j\omega)$, $P_d(j\omega)$ as power spectral densities, and the exact formulation of G is:

$$G(j\omega) = P_{ad}(j\omega)/P_d(j\omega) \tag{8}$$

where $P_{ad}(j\omega)$ is the cross-power spectral density between absolute and differential signals. According to the variable definitions,

$$D(j\omega) = H(j\omega)A(j\omega) + B(j\omega) \tag{9}$$

the power spectral density of the output is:

$$P_d(j\omega) = P_a(j\omega)\ HH^*(j\omega) + P_b(j\omega) \tag{10}$$

Assuming that $b(x)$ and $a(x)$ are uncorrelated, the cross-power spectral density is:

$$P_{ad}(j\omega) = P_a(j\omega)H^*(j\omega) \tag{11}$$

By using equations (8), (10) and (11), the inverse filter becomes:

$$G(j\omega) = \frac{1}{H(j\omega)} \frac{HH^*(j\omega)}{|H(j\omega)|^2 + P_b(j\omega)/P_a(j\omega)} \tag{12}$$

Therefore, the optimal inverse filter is the multiplication of the direct inverse filter by a regularization function depending on the noise-to-signal ratio $NS_r^2 = P_b(j\omega)/P_a(j\omega)$. If NS_r^2 tends to 0, the inverse filter tends to the direct inverse filter; if NS_r^2 tends to $+\infty$, the inverse filter tends to 0. Obviously the noise-to-signal ratio can be adjusted along the different frequencies, depending on a priori noise characteristics.

5.3 Examples of inverse filter realizations

The inverse Wiener filter is an infinite impulse response (IIR) filter, tuned with the NS_r ratio. Figure 10 presents one realization of the inverse Wiener filter with NS_r=0.1.

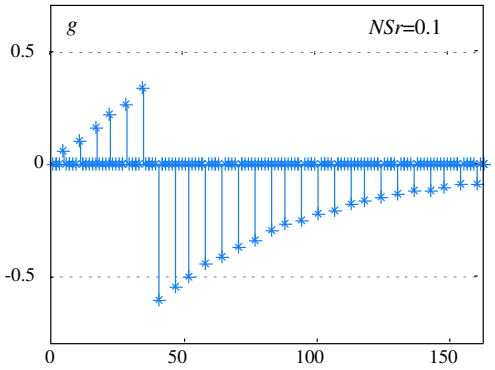

Fig. 10. example of impulse response of one inverse Wiener filter.

The inverse filter tuning requires the knowledge of the noise characteristics (white noise or colored noise, signal-to-noise ratio). Once this adjustment is carried out, the output signal can be considered as an estimation of the absolute signal. Figure 11 presents processed signatures. Note that the estimated signal is similar to an absolute one.

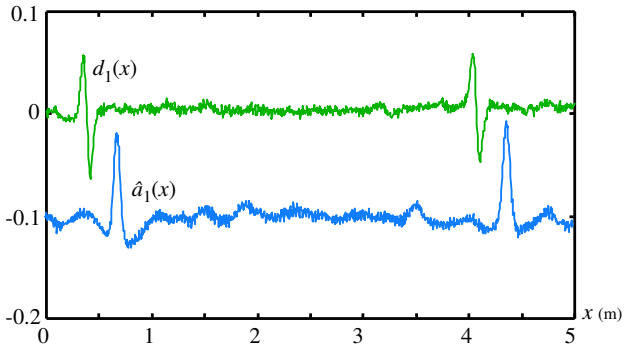

Fig. 11. two minor defects and their inversions.

Figure 12 presents the frequential behavior of direct and inverse filters for three values of NS_r ratio. The inverse filter $G(j\omega)$ tends to the direct inverse filter $1/H(j\omega)$ when the NS_r ratio becomes low.

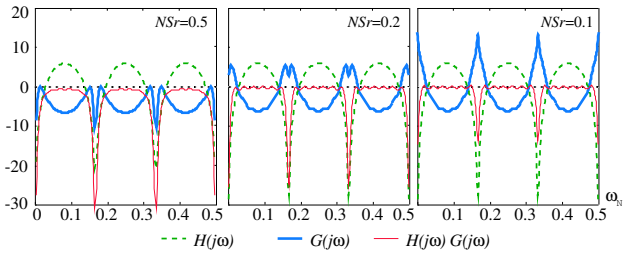

Fig. 12. frequency responses in dB for different tunings of differential measurement inversion.

5.4 Detector structure

On-line pattern recognition procedure requires two successive operations: detection and classification. The first solution consists in a detector deliberately permissively tuned [7], followed by a complete classifier including a rejection class. Following this approach, previous works have been developed with the help of neural network techniques [8].

The present results are based on a single processing which aggregates detection and classification phases and is dedicated to the minor defects (shellings and welded joints).

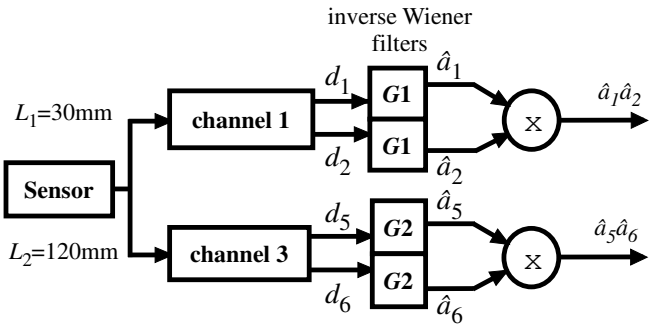

Fig. 13. enhanced detectors.

The detector structure associates four elementary detectors. Each of them processing a particular inverted signal (figure 13). These detectors are paired on in order to increase the detection contrast. Then, the final decision phase is carried out in a particular plane whose coordinates are the enhanced detectors, according to the existing expert knowledge.

The detection is validated when the curve comes into the gray zones of the pseudo-Lissajous plane (figure 14):

$$\begin{aligned}&[(\hat{a}_1\hat{a}_2 > \lambda) \cap (\hat{a}_5\hat{a}_6 > 0)]\\ \cup&[(\hat{a}_1\hat{a}_2 > 0) \cap (\hat{a}_5\hat{a}_6 > 4\lambda)]\\ \cup&[(\hat{a}_1\hat{a}_2 < -\mu) \cap (\hat{a}_5\hat{a}_6 < 0)]\\ \cup&[(\hat{a}_1\hat{a}_2 < 0) \cap (\hat{a}_5\hat{a}_6 < -4\mu)] = 1\\ &\Longrightarrow minor\ defect \end{aligned} \quad (13)$$

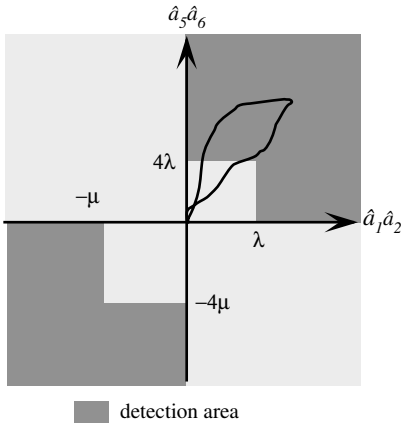

Fig. 14. detector representation.

The adjustment of the thresholds λ and μ was made with the help of ROC curve (figure 15). The optimal setting stands at the point where the distance between the ROC curve and the optimal point (0,1) is the lowest ($dist \approx 0.3$).

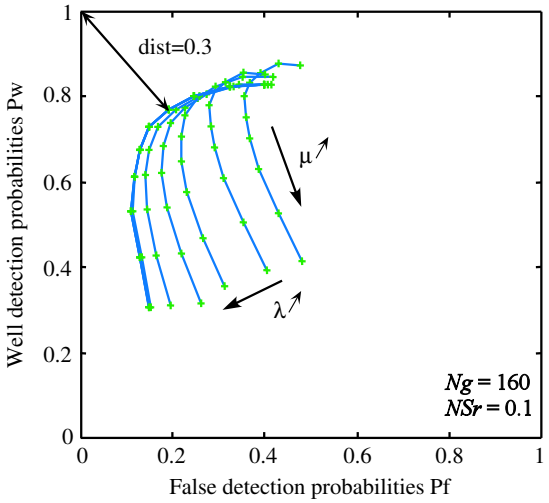

Fig. 15. ROC with enhanced Wiener inversion.

The results are similar to the wavelet detector ones. Nevertheless, contrary to wavelet detector, the enhanced Wiener detector allows the separation of shellings from welded joints: the first quarter of the plane is dedicated to the shelling detection whereas the third is dedicated to the welded joint detection. Moreover, the distributions of false detection probability and well detection probability are homogenous on the whole minor defect class (union of shelling class and welded joint class). This is due to the fact that each part of the detection area has its own threshold μ or λ.

6 Conclusion

This paper presented an original non destructive evaluation system dedicated to the rail inspection. After the presentation of the technological solution, the paper dealt with the detection of minor defects (shellings and welded joints) and presented three approaches: the first one is a time heuristic approach, using directly the differential measurements, the second one is based on wavelet decomposition, and the last one implements an inverse filtering which allows the transformation of the differential probe outputs into estimated absolute ones.

The wavelet approach gives best results, thanks to the fusion of four detectors. But this detection procedure penalizes the shelling class to the detriment of the welded joint class. On the contrary, the inverse Wiener filtering allows to define a more flexible detector structure which is able to separate shellings and welded joints. However, its practical realization requires some a priori knowledge about noise model. This knowledge is generally not easy to collect, but once it was carried out, the detection results are improved.

This work was supported by the French PREDIT organization (Interministerial land transport research and innovation program) with the coordination of RATP Company.

References

1. L. OUKHELLOU, *Parametrisation et classification de signaux en contr le non destructif. Application la reconnaissance des defauts de rails par courants de Foucault*, th se de Doctorat de l'Universite Paris XI, 1997.
2. T. STRANG, T. NGUYEN, *Wavelets and filter banks*, edited by Wellesley-Cambridge. (Wellesley MA, USA, 1996).
3. P.Y. JOUBERT, Y. LEBIHAN, D. PLACKO, Quantitative Nondestructive Evaluation **26**, (1999).
4. P. AKNIN, T. MAURIN, *Systemes multi-capteurs: diagnostic et fusion*, IC2 Instrumentation et mesure vol 2, edited by Hermes. (2000)
5. M. BENTOUMI, P. AKNIN, G. BLOCH, S. TALBI, Advances in Signal Processing for Non Destructive Evaluation of Materials **4**, 6 (2001).
6. M.H. HAYES, *Statistical digital signal processing and modeling*, edited by John Wiley. (New York, USA, 1996).
7. J. RAGOT, M. DAROUACH, D. MAQUIN, G. BLOCH, *Validation de donnees et diagnostic*, edited by Herm s.(1990)
8. L. OUKHELLOU, P. AKNIN, Neurocomputing **28**, 10 (1999).